ELSEVIER

Contents lists available at ScienceDirect

Ecotoxicology and Environmental Safety

journal homepage: www.elsevier.com/locate/ecoenv



Phthalates exposure as a risk factor for gestational diabetes mellitus: Integrated evidence from epidemiological and human liver organoids studies

Huihui Liu^{a,1}, Zhaojing Yang^{a,1}, Yaru Tian^{b,c}, Zhishen Zhuang^d, Miaoying Shi^b, Hongyang Cui^e, Xiaoning Ji^f, Yuxin Wang^g, Xiaohong Wang^b, Xiaobing Zhao^a, Xudong Jia^b, Yi Wan^c, Hui Yang^{b,d,*}, Shujing Yu^{a,**}

- ^a Zaozhuang Maternal and Child Health Care Hospital, Zaozhuang 261031, China
- b NHC Key Laboratory of Food Safety Risk Assessment, China National Center for Food Safety Risk Assessment, Beijing 100021, China
- ^c Laboratory for Earth Surface Processes, College of Urban and Environmental Sciences, Peking University, Beijing 100871, China
- d School of Public Health, Southern Medical University, Food Safety and Health Research Center, Guanezhou 510515, China
- ^e National Institute of Environmental Health, Chinese Center for Disease Control and Prevention, Beijing 100021, China
- f The Seventh Affiliated Hospital of Sun Yat-sen University, Shenzhen 518107, China
- g National Institute for Nutrition and Health, Chinese Center for Disease Control and Prevention, Beijing 102206, China

ARTICLE INFO

Edited by Renjie Chen

Keywords:
Phthalates exposure
Gestational diabetes mellitus (GDM)
Human liver organoids
Metabolic disruption
Hepatotoxicity

ABSTRACT

Gestational diabetes mellitus (GDM) poses significant risks to both maternal and child health, and its rising incidence necessitates exploration of environmental risk factors. In GDM development, the role of environmental risk factors such as phthalates, a ubiquitous class of endocrine-disrupting chemicals, is not well understood. In this study, we integrated epidemiological and toxicological studies to explore the association between phthalates exposure and GDM risk. We detected ten major phthalates metabolites in serum samples from a GDM casecontrol cohort and found that the levels of Monobutyl phthalate (MBP), Monoethylhexyl phthalate (MEHP), Monoethyl phthalate (MEP), and Monobenzyl phthalate (MBzP) were significantly elevated in GDM patients compared to healthy controls. By establishing human liver organoids model and high-content imaging method, we demonstrated that MEHP and MBP (2, 10, and 50 μ M) enhanced glucose uptake and lipid accumulation in a dose-dependent manner, promoted glycolysis, and altered key metabolic pathways related to insulin resistance. RNA sequencing and pathway analysis revealed that both MEHP and MBP (100 µM) selectively upregulated glycolysis-associated genes while suppressing other glucose metabolism pathways, such as the Tricarboxylic acid cycle and Pentose phosphate pathway, leading to increased pyruvate catabolism and lactate accumulation. Furthermore, liver organoids exhibited greater sensitivity to glucose metabolic disruption in response to MEHP than HepG2 cells, highlighting their suitability as a model for studying phthalates-induced hepatotoxicity. Our study provides novel evidence linking phthalate exposure to GDM risk and elucidates the underlying mechanisms through which phthalates disrupt hepatic metabolism.

1. Introduction

Gestational Diabetes Mellitus (GDM), a carbohydrate metabolism disorder first diagnosed during pregnancy, affects approximately 14 % of global pregnancies (Sweeting et al., 2024). Its prevalence aligns with the rising trends of obesity and Type 2 Diabetes Mellitus (T2DM), posing

a significant public health threat to maternal and child health (McIntyre et al., 2024). GDM elevates the risk of pregnancy-induced hypertension, cesarean delivery, and postpartum T2DM in pregnant women, and is closely associated with long-term health issues such as obesity and metabolic syndrome in offspring (McIntyre et al., 2019). Despite the complex pathophysiology of GDM, insulin resistance is considered one

^{*} Corresponding author at: NHC Key Laboratory of Food Safety Risk Assessment, China National Center for Food Safety Risk Assessment, Beijing 100021, China. ** Corresponding author.

E-mail addresses: yanghui@cfsa.net.cn (H. Yang), shujingyu0323@163.com (S. Yu).

¹ Authors contributed equally to this work

of the key underlying mechanisms (Hivert et al., 2024). Exposure to endocrine-disrupting chemicals (EDCs) may disrupt metabolic pathways and contribute to this process (Eberle and Stichling, 2022; Kahn et al., 2020; Yan et al., 2022). Thus, elucidating the etiology of GDM, particularly the mechanisms of environmental risk factors, is crucial for developing effective prevention and intervention strategies to reduce GDM incidence and its long-term health impacts.

Phthalates, a class of widely used EDCs, have garnered attention for their potential metabolic-disrupting effects (Huang et al., 2023; Tuculina et al., 2022). Found in plastic products, cosmetics, and medical devices, phthalates can enter the human body through diet, respiration, or skin contact (Fruh et al., 2022). Energy metabolism during pregnancy may be more sensitive to the toxic effects of phthalates (Gao et al., 2021). Emerging evidence has suggested a link between phthalate exposure and GDM. However, epidemiological studies yielded conflicting results. While some epidemiological studies found no significant association between DEHP exposure and gestational glucose intolerance or GDM (James-Todd et al., 2018; Robledo et al., 2015; Shapiro et al., 2015), others reported a decrease in the risk of gestational glucose intolerance with increased urinary DEHP concentrations in pregnant women (James-Todd et al., 2016; Martínez-Ibarra et al., 2019). On the contrary, a study of 705 pregnant women revealed a significant increase in GDM odds with interquartile range increase in early pregnancy urinary monoethyl phthalate (MEP) concentrations (Shaffer et al., 2019). Maternal serum phthalate metabolites, monobutyl phthalate (MBP) and mono-isobutyl phthalate (MIBP), were also reported to be positively correlated with GDM risk and 2-hour glucose levels (Wang et al., 2023). These discrepancies may stem from differences in exposure time windows, metabolite types, or population genetic heterogeneity (Eberle and Stichling, 2022). However, the findings of these "correlation" studies alone are insufficient to establish a causal relationship between phthalate exposure and GDM, thus cannot be readily translated into health management strategies. Therefore, toxicological investigations are imperative to elucidate the underlying mechanisms through which phthalates may induce GDM.

Previous studies have indicated that phthalates may interfere with metabolic homeostasis through multifaceted biological pathways, though the exact mechanisms by which phthalates affect GDM are not yet clear. For example, phthalates can bind to steroid hormone receptors, such as estrogen receptors (ER) and androgen receptors (AR), disrupting endogenous hormonal signaling pathways (Takeuchi et al., 2005). This interference may impair insulin sensitivity and thereby perturb glucose metabolism. In addition, dysregulation of peroxisome proliferators-activated receptors (PPARs) by DEHP can alter adiponectin secretion and promote adipose tissue remodeling, exacerbating insulin resistance and glucose intolerance (Schaffert et al., 2022). Other toxicity pathways such as oxidative stress, inflammatory responses, and epigenetic modifications have also been reported (Filardi et al., 2020; Mariana and Cairrao, 2023). Importantly, the liver, as the primary organ responsible for glucose production and insulin signaling, plays a pivotal role in regulating glucose and lipid metabolism. Dysregulation of hepatic metabolic pathways can have a profound impact on systemic glucose homeostasis (Petersen et al., 2017). Given this critical role, understanding the mechanisms by which phthalates may disrupt hepatic metabolism is essential for elucidating the etiology of GDM. However, current research on the hepatotoxicity of phthalates primarily relies on animal studies, which often lack direct human relevance due to significant interspecies differences in liver physiology. Variations in the expression and function of key metabolic enzymes and receptors, such as PPARs, can lead to different responses to phthalate exposure between animals and humans (Corton et al., 2018). This interspecies variability poses a major challenge for extrapolating the results of animal studies to human health risks. Therefore, there is a pressing need for more human-relevant models to study the metabolic-disrupting effects of phthalates. The liver organoid, an excellent model for studying hepatic energy metabolism (Hendriks et al., 2023; Huch et al., 2013), has not yet been utilized to investigate the relationship between phthalates and GDM.

In this study, we aimed to explore the association between phthalates exposure and GDM by integrating human population and toxicological studies. In the case-control study, we found that levels of phthalate metabolites MBP and MEHP were significantly elevated in GDM patients compared to healthy controls, suggesting a potential link to GDM risk. Using human liver organoids, we further demonstrated that MEHP and MBP disrupted hepatic glucose and lipid metabolism, promoting glycolysis and altering key metabolic pathways related to insulin resistance. The study highlights the suitability of liver organoids as a sensitive model for investigating the metabolic disrupting effects of phthalates and provides foundational evidence for exploring environmental interventions to reduce GDM incidence.

2. Materials and methods

2.1. Chemicals and reagents

All chemicals, antibodies, and reagents used in this study are detailed in Supplementary Table S1.

2.2. GDM cohort

This case-control study enrolled volunteers from Zaozhuang Maternal and Child Health Hospital in Zaozhuang City, Shandong Province, eastern China. A total of 200 individuals were recruited between 2023 and 2024, comprising 102 patients with gestational diabetes and 98 healthy controls. Baseline information was collected on age, gestational week, height, pre-pregnancy weight, current weight, body mass index (BMI), serum glucose level, and the oral glucose tolerance test (OGTT) result. Participants' baseline information and blood samples were collected at the hospital, where blood samples were centrifuged at 4000 rpm for 10 min to separate serum All serum samples were stored at $-80\,^{\circ}\text{C}$ until analysis. Ethical approval (NO. zfy-2023–69) for the case-control study was obtained from the Maternal and Child Health Hospital of Zaozhuang City, Shandong Province of China, and each participant provided written informed consent.

2.3. Sample processing and UPLC-MS/MS analysis

Following a period of overnight thawing at 4°C, 0.5 mL of serum was extracted and combined with 250 μl of ammonium acetate buffer (1 M, pH 6.7), 5 μl of a mixed plastocyanin internal standard solution (MEP-d4, MIBP-d4, MCHP-d4, MBP-d4, and MEHP-d4), as well as 30 μl of β -glucuronidase/aromatic sulphate lyase. They were vortexed to mix well and then incubated in a temperature chamber set at 37°C for 12 h in dark. Subsequently, the reaction was terminated by the addition of 1 mL of phosphate buffer (0.1 M, pH 1.9). The Oasis Prime HLB column was activated with methanol (6 mL) and phosphate buffer (6 mL), followed by the addition of the incubated sample for separation. The retained extracts were then dried under a gentle stream of nitrogen for 20 min, after which the extracts were eluted from the columns with 0.5 mL of methanol. All eluates were stored at -20°C until the samples were assayed.

Chromatographic separation and determination of the targeted compounds were performed on an ACQUITY Ultra Performance LC I-Class system and a Waters XEVO-TQ-XS triple quadrupole mass spectrometer equipped with an ESI source. UPLC was carried out on a Poroshell 120 HPH C18 column (2.1 \times 100 mm, 1.9 μm ; Agilent). The temperatures of column and sampler were maintained at 35 °C and 8 °C, respectively. The mobile phase, operating at a flow rate of 0.3 mL/min, consisted of Milli-Q water containing 0.1 % acetic acid as solvent A and methanol as solvent B. The injection volume was 2 μL . The gradient elusion began at 10 % B and was held for 1 min, and then increased to 45 % B at 1.5 min and was held for 2.5 min. After that, mobile phase B

increased to 100 % at 10 min. After that the column was washed with 100 % A for 3 min, then the column was re-equilibrated with the initial mobile phase composition for 2 min before the next injection.

The ESI-MS/MS was operated in a negative mode. Nitrogen and argon were used as the desolvation gas and the collision gas, respectively. The conditions for mass detection were optimized to obtain the highest signal intensity: capillary voltage, 2.5 KV; desolvation temperature, 500 $^{\circ}$ C; source temperature, 150 $^{\circ}$ C; desolvation gas flow rate, 1200 L/h; cone gas flow rate, 150 L/h. The data were obtained and analyzed using Waters MassLynx v4.2 software (Micromass,

Manchester, UK). Quantitative analysis of the THs was performed with multi-selected reaction monitoring (MRM). In the MRM transitions, the dwell times were automatically selected. The baseline separation and accurate quantification of the target phthalate metabolite isomers (including MBP & MIBP, MEHP & MOP, and MNP & MINP) were validated (Supplementary Figure S2). Blank controls were incorporated during sample detection process (Supplementary Figure S3).

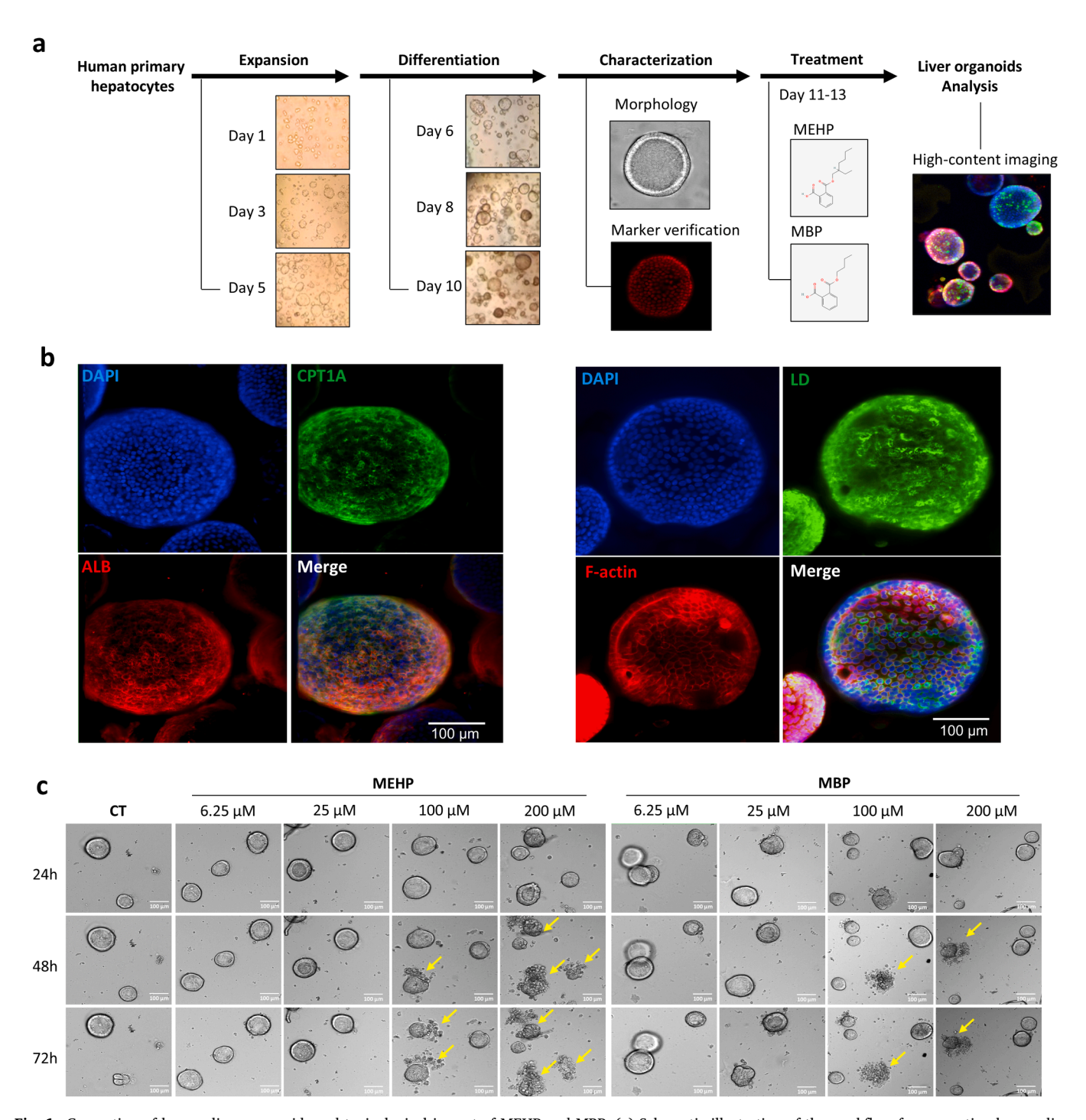


Fig. 1. Generation of human liver organoids and toxicological impact of MEHP and MBP. (a) Schematic illustration of the workflow for generating human liver organoids and application for toxicological study of phthalates. (b) Immunofluorescence staining of mature hepatocyte marker proteins (CPT1A and ALB) and lipid droplets (LD) within organoid cells after 5 days of differentiation. (c) Dose- and time- dependent toxicity of MEHP and MBP on liver organoids. Representative bright-field images showing the structural alterations of liver organoids treated with MEHP and MBP at various concentrations (0, 6.25, 25, 100, 200 μ M) for 24–72 h.

2.4. Quantitation of phthalate metabolites

The ten phthalate metabolites, including Monobutyl phthalate (MBP, CAS: 131-70-4), Monoethylhexyl phthalate (MEHP, CAS: 4376-20-9), Monoethyl phthalate (MEP, CAS: 2306-33-4), Monoisobutyl phthalate (MIBP, CAS: 30833-53-5), Monononyl Phthalate (MNP, CAS: 24539-59-1), Monobenzyl phthalate (MBzP, CAS: 2528-16-7), and Monocyclohexylphthalate (MCHP, CAS: 7517-36-4), Monooctyl phthalate (MOP, CAS: 5393-19-1), Monodecyl Phthalate (MDP, CAS: 24539-60-4), and Monoisononyl phthalate (MINP, CAS: 106610-61-1) were quantified using Waters MassLynx v4.2 software (Micromass). Charcoal-stripped human serum with no detectable level of any phthalate metabolite was used to prepare the quality control samples and calibration curve samples. To obtain calibration curves to determine the phthalate metabolites, the working standard solution was diluted to concentrations of 0.1, 0.2, 1, 2, 5, 10, 20, 50, 100, and 200 μ g/ L for LC-MS/MS analysis. The calibration curves were obtained by plotting the area ratios of each analyte relative to its internal standard versus the respective concentration ratios, and the relationship was fitted using linear regression. The concentration of each phthalate metabolite in a serum sample was interpolated using this linear function. The analytes were identified on a comparison of the retention time and the ratio of the two selected MRM ion transitions with those of the standards. To ensure the accuracy of the quantitative analyses, deuterium-labeled phthalate metabolites were used as internal standards. The method detection limits (MDLs) and quantification limits (MQLs) were estimated based on the peak-to-peak noise of the baseline near the analyte peak obtained by analyzing phthalate metabolite-spiked charcoalstripped human serum samples. The MDLs and MQLs were determined as the concentrations with minimum signal-to-noise (S/N) ratios of 3 and 10, respectively. Furthermore, ion suppression, accuracy, and precision analysis were also evaluated in this study.

2.5. Liver organoids

Human hepatocyte organoid lines were obtained from Beijing Daxiang Biotech. The hepatic organoids were mixed with proliferation medium (Daxiang Biotech, HG100101) containing collagen at a 1:2 ratio (v/v), and 50 μ L of the mixture (approximately 500–1000 cells per well) was seeded into 48-well plates. After solidification at 37°C for 10 min, 300 μL of proliferation medium supplemented with 0.1 % anti-apoptotic factor (Daxiang Biotech, IA100101) was added to each well. Organoids were cultured for 6-8 days with medium replacement every 3 days (Fig. 1a). For cell subculture, organoids were dissociated into small clusters (1-5 cells) using dissociation reagent (Daxiang Biotech, KC100142). The reaction was terminated by adding two volumes of wash buffer (Daxiang Biotech, KC100141), followed by centrifugation at 400 g for 5 min at 4°C. The cell pellet was resuspended in cold proliferation medium containing 2/3 collagen and replated. All steps were performed at 4°C to prevent collagen polymerization. For organoid differentiation, when organoids reached 100-200 µM in diameter, the proliferation medium was replaced with differentiation medium (Daxiang Biotech, HD100101). After 3-5 days of culture, mature parenchymal organoids were obtained. The maturation of liver organoids was confirmed by immunofluorescence staining using antibodies against CPT1A and ALB.

2.6. Treatment of liver organoids

Two representative phthalate metabolites (MBP and MEHP) that exhibit higher exposure levels compared to other metabolites detected in the serum of GDM population were selected for treatment of liver organoids. According to the average serum concentrations of MBP (412 ng/mL, corresponding to 1.86 μM), the treatment concentrations were set as 2, 10, and 50 μM in the experiments for lipid accumulation, glucose uptake, and protein expression analyses. Stock solutions of MBP

and MEHP in this experiment were prepared using dimethyl sulfoxide (DMSO), and the final DMSO concentration in all treatment groups was controlled below 0.1 %. A solvent control group was established simultaneously. Each concentration was tested in at least two replicate wells, with data collected from a minimum of 10 organoids per well. To determine cytotoxicity, mature organoids were seeded into 96-well plates and treated with MBP or MEHP (6.25, 25, 100, 200 μ M) for 24, 48, or 72 h. Bright-field images were acquired using ImageXpress Micro confocal system. Cell viability was quantitatively analyzed with 7-aminoactinomycin D (7-AAD) staining.

2.7. Glucose uptake

Organoids were gently collected into Eppendorf tube using precooled cleaning solution. Organoid pellets were obtained after centrifugation at 400 g for 5 min at 4 °C and then washed twice with PBS (Gibco, C10010500BT) by shaking at 40 rpm for 5 min each time. A 250 μM 2-NBDG probe (Thermo Scientific, N13195) was added, and the samples were incubated in an incubator for 12 h. After the incubation period, the samples were washed twice by shaking with PBS. Subsequently, the cell nuclei were labeled with Hoechst 33342 (Solarbio, C0031) from a 10 $\mu g/mL$ solution. Following a single wash by shaking with PBS, the organoid pellets were resuspended in FluoroBrite DMEM and transferred to a 96-well black plate (in vitro scientific, 060096) for imaging analysis.

2.8. Lipid droplets staining

The organoids were collected and washed using the same procedure described previously. Sedimented organoids were fixed in 4 % Paraformaldehyde at room temperature (RT) for 1 h. Then washed twice with PBS and incubated with labeled lipid (LD) probes (Thermo Scientific, D3922, 1 $\mu g/mL)$ and Hoechst 33342 in PBS for 30 min at room temperature, protected from the light.

2.9. Antibodies staining

Organoids were collected, washed, and fixed as previously described. Then fixed organoids were first washed twice with PBS and then simultaneously blocked and permeabilized using 5 % BSA (Solarbio, SW3015) and 0.3 % Triton-X100 (Sigma-Aldrich, X100-500 mL) in PBS at RT for 1 h. Organoids were washed once with 0.5 % BSA-PBS and subsequently incubated with primary antibodies in 2.5 % BSA-PBS overnight at 4 °C. The primary antibodies used were: CPT1A Polyclonal antibody (Proteintech, 5184-1-AP), Albumin Polyclonal antibody (Proteintech, 16475-1-AP), HK2 Mouse Monoclonal Antibody (Biodragon, BD-PA0088), PFKFB3 (11K15) Rabbit Monoclonal Antibody (Biodragon, RM5591), G6PC Polyclonal Antibody (Thermo Scientific, PA542541), Perilipin-2 Mouse Monoclonal Antibody (EbioCell, EAB22501), GAPDH Mouse Monoclonal Antibody (EbioCell, EAB21667) and LDHA (4H19) Rabbit Monoclonal Antibody (Biodragon, RM6092), all primary antibodies dilutions were 1:100. After three washes with 0.5 % BSA-PBS, organoids were incubated with appropriate Alexa Fluor secondary antibodies and Alexa Fluor 555 Phalloidin (CST, 8953S) (1:200) in 2.5 % BSA-PBS for 2 h at RT. The secondary antibodies used were: Anti-mouse IgG (H+L), F(ab')2 Fragment (Alexa Fluor® 488 Conjugate) (CST, 4408S), Anti-rabbit IgG (H+L), F(ab')2 Fragment (Alexa Fluor® 647 Conjugate) (CST, 4414S), all secondary antibodies dilutions were 1:500. Then Organoids were washed once with 0.5 % BSA-PBS, after which they were incubated with Hoechst 33342 (1:100) in 0.5 % BSA-PBS for 20 min at RT and washed once more with 0.5 % BSA-PBS.

2.10. HCI quantitative analysis

The stained organoids were gently washed with PBS and then

captured on the ImageXpress Micro Confocal system (Molecular Devices). The images were processed and analyzed using MetaXpress software (Version 6.5, Molecular Devices). Briefly, Optical sections were diligently acquired at intervals of 20-30 layers and 15-20 µm along the z-axis for the 3D reconstruction of 20X objectives. And then the superimposed images were synthesized into 2D projection images, converted into binary images. We used the MetaXpress software to add the "Top Hat" mask to the corresponding fluorescence channel to make the features of the organoid more obvious and then set the appropriate fluorescence threshold to identify the positive staining area. Then add a "Gaussian Filter" mask, set the appropriate parameters to make the internal brightness of the organoids uniform, so as to facilitate the identification of organoid spheres. Finally, "Find Round Objects" Mask and "Find Blobs" Mask are added to identify organoids and the number of nuclei in them. Parameters including DAPI Features Count and ORG Area Sum were exported. Fluorescence quantification was determined by using the formula: MSA= $\frac{ORG Area Sum (\mu m^2)}{DAPI Features Count}$.

2.11. RNA sequencing

Mature hepatocyte organoids cultured in 24-well plates were treated with 100 μM MEHP and MBP for 48 h, respectively. HepG2 cells were cultured in 6-well plates were treated with 100 µM MEHP and MBP for 72 h, respectively. The total RNA was extracted from the organoids and HepG2 cells with TRIzol. The RNA sequencing was kindly executed by Novogene Biotech Co., Ltd. (Beijing, China). The RNA integrity was meticulously assessed using the RNA Nano 6000 Assay Kit of the renowned Bioanalyzer 2100 system (Agilent Technologies, Santa Clara, CA, USA). A differential expression analysis of the groups was expertly conducted using the R package "DESeq2" (1.20.0). We identified differentially expressed genes (DEGs) by utilizing DESeq2 with a p value < 0.05 and |log2 (Fold Change)| > 1 (Jabato et al., 2021). A Kyoto Encyclopedia of Genes and Genomes (KEGG) pathway analysis of the DEGs was performed using the STRING online analysis tool (https://cn. string-db.org/, accessed on 10 September 2024). A gene set enrichment analysis (GSEA) exercise was conducted locally utilizing the recent version of the established GSEA analysis software (http://www.broa dinstitute.org/gsea/index.jsp, accessed on 1 August 2024). Raw data are available in the Gene Expression Omnibus database (https://www. ncbi.nlm.nih.gov/geo/) with the accession numbers GSE293605.

2.12. Determination of Lactate and Pyruvate

Lactate and Pyruvate concentrations of culture medium levels were measured using L-Lactate Assay Kit with WST-8 (Beyotime, S0208S) and Amplex Red Pyruvate Assay Kit (Beyotime, S0299S) according to the manufacturer's instruction.

2.13. Statistical analysis

In the epidemiological study, descriptive analyses and the basic characteristics of the study population were performed. The Mann-Whitney U test was used for variables that still did not conform to normality after the Log transformation, and the independent samples t test was used for variables that conformed to normality after the Log transformation. The data analyses were performed using GraphPad Prism 10.1 (GraphPad Software Inc., San Diego, CA, USA) and IBM SPSS Statistics for Windows (Version 26.0. Armonk, NY). The data are expressed as the mean \pm standard deviation (SD). Statistical analyses between multiple groups were performed using the one-way analysis of variants (ANOVA), followed by Bonferroni's test multiple comparisons. The level of statistical significance was set at p < 0.05.

3. Results

3.1. Association between phthalates exposure and gestational diabetes mellitus (GDM)

In the case-control study, we carefully balanced the sample size, age, height, weight, and other parameters between the GDM group and the control group, thereby effectively controlling for the impact of other confounding factors (Table 1). Additionally, we focused on the extraction and analysis of phthalates metabolites as the sole target in the serum samples, ensuring the accuracy of the analysis. These methodological strengths provide a more precise assessment of the association between phthalates exposure and GDM risk.

Among ten major phthalates metabolites, MBP, MEHP, and MIBP were universally detected (100 % detection rate), while MEP was identified in 98.5 % of samples. MCHP and MBZP exhibited moderate detection rates of 55 % and 27.5 %, respectively, whereas the remaining metabolites (MNP, MDP, MINP, MOP) were detected at frequencies below 5 %. MBP demonstrated the highest mean serum concentration ($\sim 400~\rm ng/mL$), followed by MEHP ($\sim 10~\rm ng/mL$), while all other metabolites exhibited average concentrations below 2.5 ng/mL. No significant differences were observed between the case and control groups regarding age, height, weight, or body mass index (BMI) (Table 1). However, the serum levels of MBP, MEHP, MEP, and MBZP were significantly elevated in the GDM group compared to healthy controls (Table 1). These findings suggest that internal phthalate exposure is associated with GDM incidence.

3.2. Impact of phthalate metabolite MEHP and MBP on human liver organoids

The potential impacts of MEHP and MBP on glucose and lipid metabolism were examined using human liver organoids derived from primary human hepatocytes. Human primary hepatocytes were

Table 1Characteristics of participants and phthalates exposure levels in the GDM case-control study.

Index	Control group (n = 98)	GDM group $(n = 102)$	P value
Age (year)	31.0 (27.8–34)	32.0 (29.0-35.0)	0.09
Height (cm)	163.0 (160.0-166.0)	162.0 (159.8-166.3)	0.26
Body weight (kg)	69.1 (62.0–77.1)	72.0 (65.0–79.1)	0.14
BMI (kg/m ²)	22.8 (20.6-25.5)	23.8 (21.2-26.6)	0.07
Serum Glucose	4.7 (4.6-4.9)	5.2 (4.9-5.2)	<
(mmol/L)			0.001***
OGTT (mmol/			
L)			
0 h	4.3 (4.1-4.6)	4.9 (4.5-5.2)	<
			0.001***
1 h	7.2 (6.2-8.2)	10.1 (9.0-10.7)	<
			0.001***
2 h	6.2 (5.5-7.0)	8.6 (7.3-9.4)	<
			0.001***
Phthalates metal	bolites (ng/mL)		
MBP	396.34	412.46	0.0333 *
	(313.06-558.17)	(328.45-622.05)	
MEHP	9.37 (7.42-12.75)	11.87 (9.19-15.68)	<
			0.001***
MIBP	2.03 (1.47-2.84)	1.79 (1.20-2.61)	0.058
MEP	0.62 (0.50-0.96)	0.83 (0.64-1.12)	<
			0.001***
MCHP	0.05 (0.01-0.13)	0.03 (0.01-0.13)	0.154
MBzP	0.02 (0.02-0.02)	0.02 (0.02-0.07)	<
			0.001***

Variables were reported as median (interquartile range). Data was analyzed using the Mann-Whitney U test or Independent Samples t-test. Statistical significance is indicated in comparison to the control group, with * p < 0.05, ** p < 0.01, and *** p < 0.001.

expanded and differentiated into liver organoids, which were subsequently characterized (Fig. 1a). After 5 days of differentiation, immunofluorescence staining demonstrated the robust expression of mature hepatocyte marker proteins, including CPT1A and ALB, while LD was readily visualized within the organoid cells (Fig. 1b). Morphological analysis revealed that treatment with MEHP and MBP at concentrations exceeding 100 μ M induced significant structural alterations and collapse of liver organoids. The cytotoxicity also exhibited time-dependent characteristics (Fig. 1c). Staining with 7-AAD also indicated that MEHP (200 μ M) induced significant cytotoxicity in liver organoids (Supplementary Figure S4a and b). In contrast, neither compound caused cytotoxicity at higher concentrations in HepG2 hepatoma cell line (Supplementary Figure Sc). These findings suggest that liver organoids provide a sensitive model for evaluating the toxicological effects of MEHP and MBP.

3.3. MEHP and MBP enhanced glucose uptake and lipid accumulation in human liver organoids

To evaluate the metabolic effects of MEHP and MBP in liver organoids, a high-content analytical platform based on 3D organoid imaging was developed, enabling precise identification of organoid cells and quantitative analysis of the fluorescence staining (Fig. 2a). Using this approach, the effects of lower concentrations of MEHP and MBP (2, 10, 50 μ M) on glucose and lipid metabolism were systematically assessed. The results showed that treatment with MEHP and MBP significantly increased the mean stain area (MSA) of the glucose probe (2-NBDG) in a dose-dependent manner (Fig. 2b); the effect in the MBP group was

relatively weaker, but statistically significant compared to the control group (Fig. 2b). Similarly, lipid accumulation was examined using LD probe staining. Consistent with the glucose uptake results, MEHP treatment caused a dose-dependent increase in LD levels within liver organoids, while MBP treatment also led to significant elevations in lipid accumulation compared to controls (Fig. 2c). These findings indicate that both MEHP and MBP disrupt glucose and lipid metabolism in liver organoids, potentially contributing to metabolic dysfunction in hepatocytes.

3.4. MEHP and MBP upregulated insulin resistance associated signaling pathways

To elucidate the mechanisms by which MEHP and MBP disrupt energy metabolism, RNA sequencing analysis was conducted using liver organoids. The results revealed a significant overlap in gene expression changes induced by MEHP and MBP, with over 64 % of the affected genes shared between the two compounds (Fig. 3a). Pathway enrichment analysis identified glycolysis/gluconeogenesis and the HIF-1 signaling pathway as the most significantly altered KEGG pathways (Fig. 3b). A strong positive correlation was observed between the upregulated and downregulated genes in response to MEHP and MBP treatment (Fig. 3c). For example, both compounds significantly upregulated glycolysis-associated genes (HK2, PFKFB3, PCK2, ALDOC, ENO2, PKM, etc.), while downregulating cell cycle- and mitosis-associated genes (CCNA2, CCND1, CCNB2, MKI67, CDC45, CENPF, MCM10, etc.) (Fig. 3c). Gene set enrichment analysis (GSEA) further showed that MEHP and MBP significantly upregulated pathways related

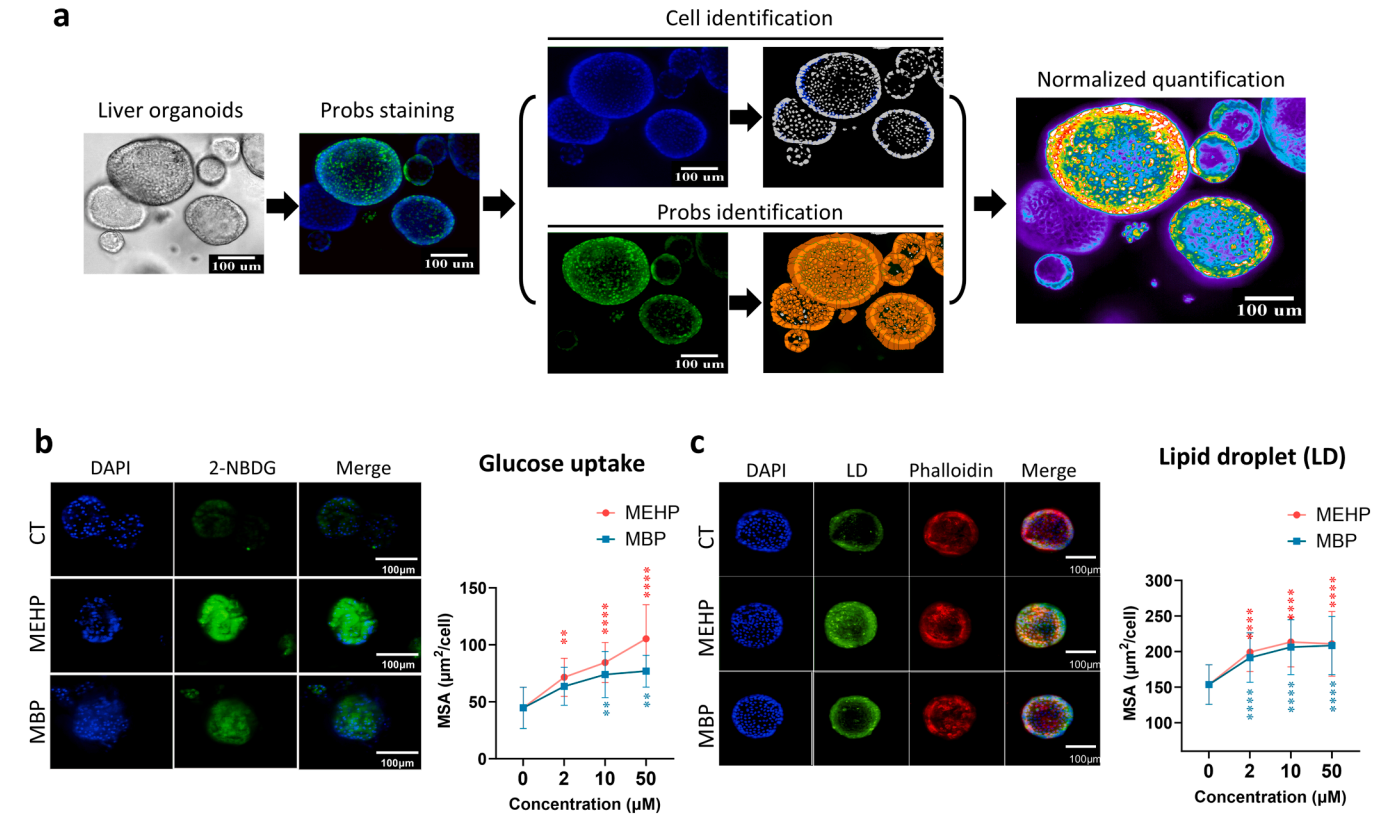


Fig. 2. Effects of MEHP and MBP on glucose uptake and lipid accumulation in liver organoids. (a) Schematic illustration of the prob staining, high content imaging (HCI), and quantitative analysis with the human liver organoids model. (b) Representative HCI images and quantitative analysis of the effects of MEHP and MBP on glucose uptake in liver organoids. (c) Representative HCI images and quantitative analysis of the effects of MEHP and MBP on lipid accumulation in liver organoids. Human liver organoids were treated with MEHP and MBP (2, 10, 50 μ M) for 48 h. Each concentration was tested in at least two replicate wells, with data collected from a minimum of 10 organoids per well. Error bars represent the mean \pm standard deviation (SD) of results from three independent experiments. The mean stain area (MSA) of staining was normalized by cell counting in each organoid. Data were analyzed using one-way ANOVA followed by Dunnett's multiple comparisons test. Statistical significance is indicated in comparison to the control group, with *p < 0.05, **p < 0.01, ***p < 0.001, and ****p < 0.0001.

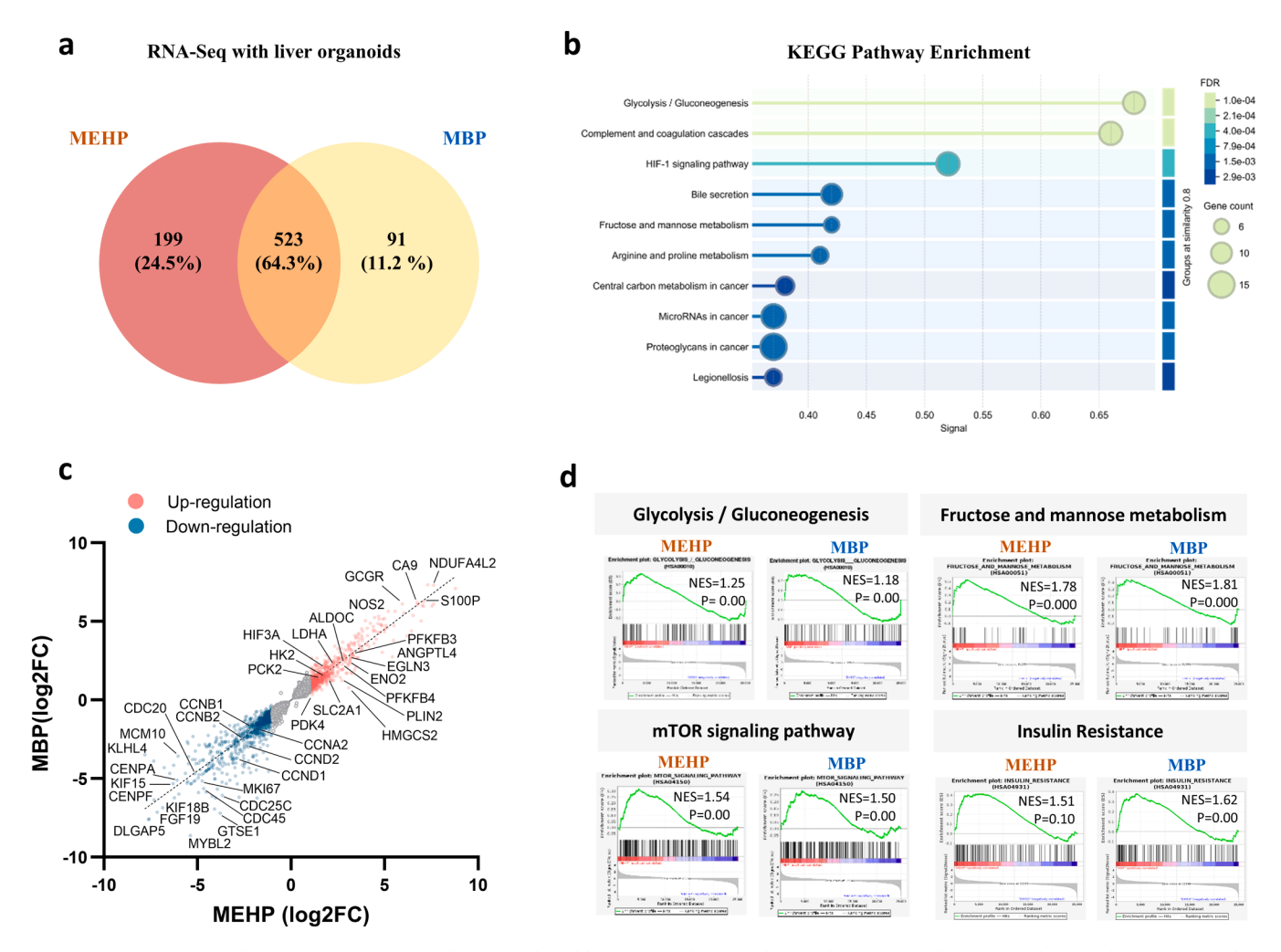


Fig. 3. RNA-sequencing analysis of gene expression changes induced by MEHP and MBP in human liver organoids. (a) Venn diagram showing the overlap in differentially expressed genes (DEGs) between MEHP- and MBP-treated liver organoids. (b) KEGG pathway enrichment analysis of the DEGs. The top 10 significantly altered pathways are displayed. (c) Correlation of upregulated (red) and downregulated (blue) genes in response to MEHP and MBP treatment. (d) GSEA analysis highlighting the significantly enriched pathways related to glycolysis/gluconeogenesis, fructose and mannose metabolism, mTOR signaling pathway, and insulin resistance.

to "glycolysis/gluconeogenesis" and "fructose and mannose metabolism" (Fig. 3d). Additionally, pathways closely associated with metabolic disorders and diabetes, such as the "mTOR signaling pathway" and "insulin resistance", were markedly upregulated in MEHP- and MBP-treated groups (Fig. 3d). These findings suggest that MEHP and MBP selectively disrupt the balance between glycolysis and gluconeogenesis in liver organoids, potentially inducing insulin resistance through activation of key signaling pathways linked to metabolic disorders.

3.5. MEHP and MBP selectively enhanced glycolysis in human liver organoids

Next, we utilized transcriptomic data to analyze the specific impact of MEHP and MBP on glucose metabolism in liver organoids. Initially, we observed that the expression levels of genes related to glycolysis/gluconeogenesis and insulin resistance were significantly altered following treatment with MEHP and MBP (Fig. 4a). Notably, the expression levels of glycolysis-related genes were significantly upregulated, while the expression levels of key rate-limiting enzymes in gluconeogenesis were significantly downregulated. For instance, G6PC3 (which hydrolyzes glucose-6-phosphate to glucose) and G6PD (which catalyzes the rate-limiting step of the oxidative pentose-phosphate pathway) were downregulated. Additionally, the majority of genes in

the HIF-1 signaling pathway were upregulated, indicating that MEHP and MBP promoted glycolysis while inducing the activation of the hypoxia signaling pathway. Compared to the enhancement of glycolysis, the expression levels of genes related to the Tricarboxylic acid (TCA) cycle in mitochondria and Pentose phosphate pathway were significantly downregulated (Fig. 4b). These results suggest that MEHP and MBP selectively enhance anaerobic glycolysis while suppressing other glucose metabolism pathways, including aerobic TCA cycle and Pentose phosphate pathway. Regarding lipid metabolism-related pathways, genes involved in fatty acid metabolism, fatty acid degradation, and fatty acid elongation also exhibited some changes, but the extent of these changes were moderate compared to those in glucose metabolismassociated genes (Fig. 4c). Genes related to fatty acid activation (ACSL1/ 4), triglyceride synthesis (AGPAT2, DGAT2, GPD1), and lipid droplet packaging (PLIN2) were upregulated, which may be an important factor in the lipid accumulation induced by MEHP and MBP in liver organoids.

To further validate the disturbing effects of MEHP and MBP on glucose metabolism, the expression levels of key metabolic enzymes involved in glycolysis (HK2, PFKFB3, and G6PC) were simultaneously quantified using high-content analysis (Fig. 4d). HK2 phosphorylates glucose to produce glucose-6-phosphate, the first step in glucose metabolism pathways. PFKFB3 is a bifunctional protein involved in both the synthesis and degradation of fructose-2,6-bisphosphate, and G6PC is responsible for glucose production in the terminal step of glycogenolysis

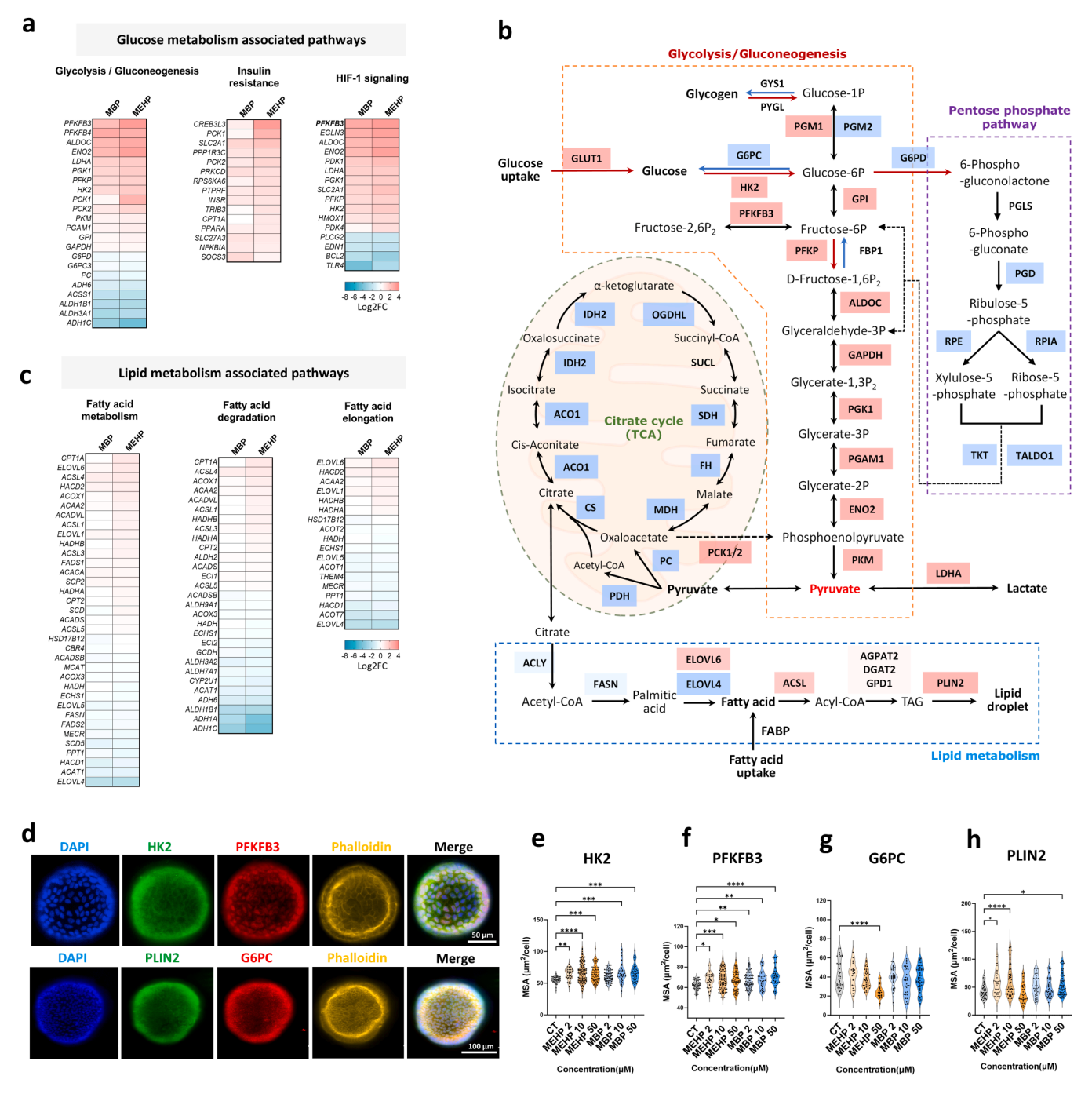


Fig. 4. Effects of MEHP and MBP on metabolism-associated gene expression profiles in human liver organoids. (a) Heatmap showing the expression change levels of genes in glucose metabolism associated pathways after treatment with MEHP and MBP. (b) Schematic illustration of disruptive effects of MEHP and MBP on cellular metabolism in the human liver organoids. Expression changes were mapped onto key genes involved in Glycolysis/Gluconeogenesis, Tricarboxylic acid cycle (TCA), Pentose Phosphate Pathway, and Lipid Metabolism. Upregulation is indicated by red boxes, while downregulation is indicated by blue boxes. (c) Heatmap showing the expression change levels of genes in lipid metabolism associated pathways after treatment with MEHP and MBP. (d) Representative high-content images showing the expression of key metabolic enzymes (HK2, PFKFB3, G6PC, and PLIN2) at the protein level in human liver organoids. (e-h) Quantification of protein expression levels of HK2 (e), PFKFB3 (f), G6PC (g), and PLIN2 (h). Human liver organoids were treated with MEHP and MBP (2, 10, 50 μ M) for 48 h. Each concentration was tested in at least two replicate wells, with data collected from a minimum of 10 organoids per well. The mean stain area (MSA) was normalized by cell counting in each organoid. Data were analyzed using one-way ANOVA followed by Dunnett's multiple comparisons test. Statistical significance is indicated in comparison to the control group, with * p < 0.05, ** p < 0.01, *** p < 0.001, and **** p < 0.0001.

and gluconeogenesis. The results demonstrated that the protein expression levels for HK2 (Fig. 4e) and PFKFB3 (Fig. 4f) in liver organoids treated with MEHP and MBP increased in a dose-dependent manner. In contrast, the protein levels of G6PC were significantly reduced following MEHP treatment (Fig. 4g). Additionally, PLIN2 expression was elevated by MEHP and MBP, but no significant dose-

response correlation was observed (Fig. 4h). Overall, these findings indicate that the effects of MEHP and MBP on intracellular carbohydrate and lipid metabolism may primarily manifest as the promotion of glycolysis.

3.6. MEHP and MBP promoted pyruvate catabolism and lactate accumulation in liver organoids

In contrast to the promotion of glycolysis, "Pyruvate metabolism" pathway was significantly down-regulated by MEHP and MBP in liver organoids, as shown by the GSEA result using RNA-seq data (Fig. 5a). Consistent with this, genes involved in pyruvate production within the pyruvate metabolism pathway, such as PCK1/2 and PKM, were significantly up-regulated, whereas most genes regulating pyruvate catabolism were consistently down-regulated (Fig. 5b). For instance, the gene expression of PC (which catalyzes the conversion of pyruvate to oxaloacetate) and PDH (that catalyzes the overall conversion of pyruvate to acetyl-CoA, providing the primary link between glycolysis and TCA cycle) were significantly decreased by MEHP and MBP. However, the expression of LDHA, which catalyzes the conversion of pyruvate to lactate with the concomitant oxidation of NADH to NAD in anaerobic glycolysis, was increased. Thus, we hypothesized that this metabolic

disruption may ultimately lead to pyruvate catabolism and lactate accumulation (Fig. 5c). To test this hypothesis, we determined LDHA expression in liver organoids at the protein level using the HCI method (Fig. 5d). HCI quantification results showed that MEHP and MBP (50 μ M) significantly elevated LDHA levels (Fig. 5e). Furthermore, the concentration of pyruvate and lactate in the culture medium of liver organoids were measured. The results indicated that the two phthalate metabolites dose-dependently decreased pyruvate levels (Fig. 5f). In contrast, lactate concentrations were significantly increased by MEHP and MBP (50 μ M) (Fig. 5g). Taking together, these results suggest that MEHP and MBP promote the metabolism of pyruvate to lactate in human liver organoids.

Collectively, the expressions of glycolytic genes (e.g., HK2, PFKFB3) were upregulated by MEHP and MBP, while the expression of genes associated with the tricarboxylic acid (TCA) cycle and pentose phosphate pathway (PPP) were inhibited. These changes drive a shift in glucose metabolism toward anaerobic glycolysis in human hepatic

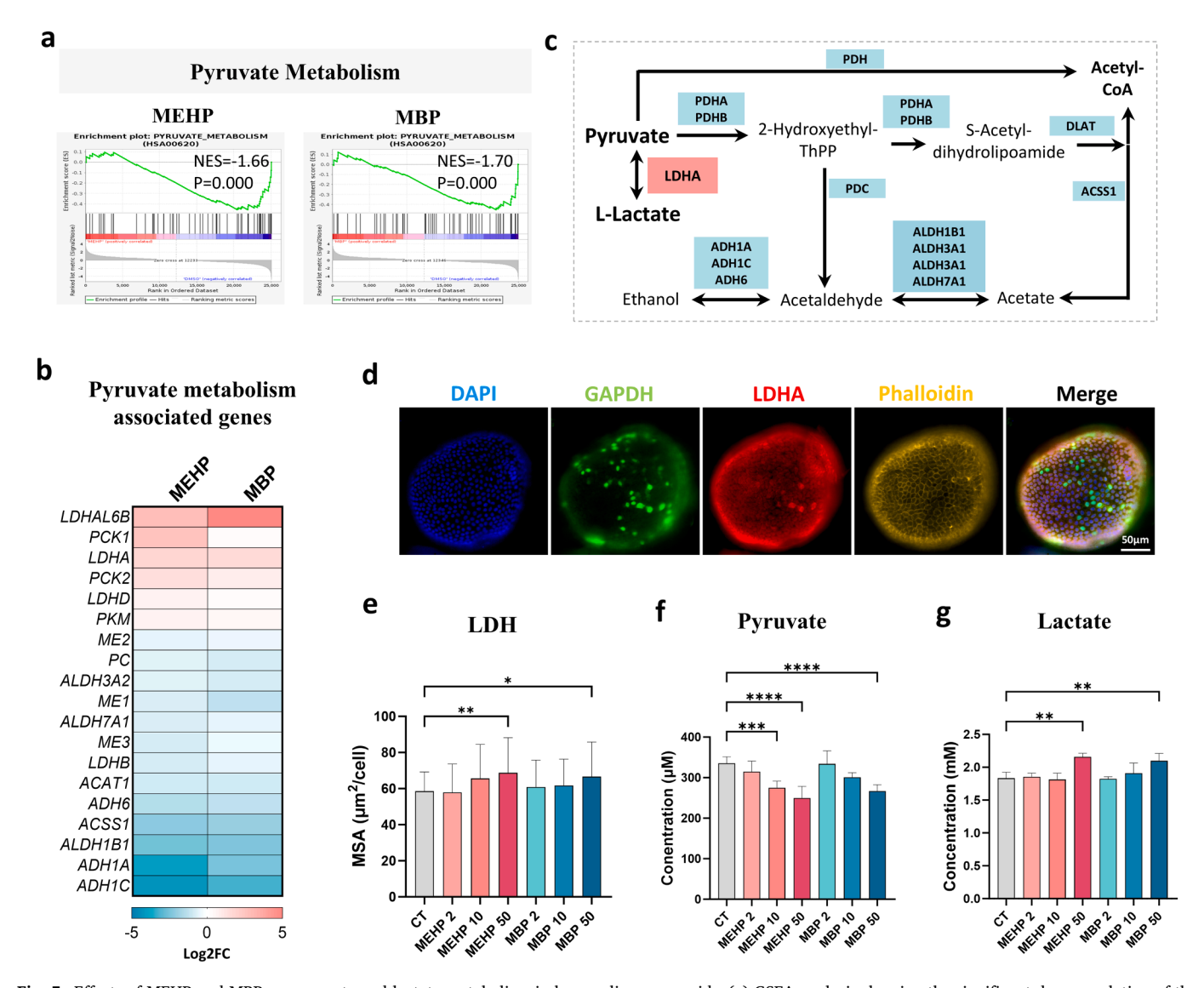


Fig. 5. Effects of MEHP and MBP on pyruvate and lactate metabolism in human liver organoids. (a) GSEA analysis showing the significant downregulation of the "Pyruvate metabolism" pathway in liver organoids treated with MEHP and MBP. (b) Relative expression levels of genes involved in pyruvate production and catabolism. (c) Schematic diagram illustrating the metabolic disruption leading to pyruvate catabolism and lactate accumulation. Upregulation is indicated by red boxes, while downregulation is indicated by blue boxes. (d) Representative immunofluorescence images of LDHA expression in liver organoids. (e) Quantification of LDHA protein expression levels. (f-g) Concentrations of pyruvate (f) and lactate (g) in the culture medium of liver organoids treated with MEHP and MBP. Human liver organoids were treated with MEHP and MBP (2, 10, 50 μ M) for 48 h. Each concentration was tested in at least two replicate wells. Data are presented as mean \pm SD from three independent experiments. Data were analyzed using one-way ANOVA followed by Dunnett's multiple comparisons test. Statistical significance is indicated in comparison to the control group, with * p < 0.05, ** p < 0.001, *** p < 0.001, and **** p < 0.0001.

organoids, leading to substantial lactate accumulation. Notably, this was in line with accumulating evidence that has established lactate as a key trigger mediating obesity-induced inflammation and systemic insulin resistance (Lin et al., 2022).

3.7. Differential responses of human liver organoids and HepG2 cell line to MEHP

Finally, we compared the responses of liver organoids and the HepG2 hepatoma cell line to the representative metabolite MEHP. RNA-sequencing analysis demonstrated that the number of genes with altered expression induced by MEHP was significantly higher in organoids (669) than in HepG2 cells (105), with only 4 overlapping genes, representing merely 0.5 % of all differentially expressed genes (Fig. 6a). Pathway enrichment analysis of the differentially expressed genes from the HepG2 cell model failed to identify any significantly enriched KEGG pathways. Additionally, the expression changes of insulin resistance-associated genes in HepG2 cells were markedly less pronounced than

those in liver organoids (Fig. 6b), suggesting that liver organoids may exhibit greater sensitivity to the metabolic disrupting effects of phthalate metabolites.

GSEA result revealed that MEHP significantly upregulated the PPAR signaling pathway in both liver organoid and HepG2 cells (Fig. 6c). However, the magnitude of alterations in PPAR signaling pathway-related gene expression were more substantial in liver organoids than in the HepG2 cell line (Fig. 6d). Notably, MEHP exerted different effects on metabolic pathways in the two models. In liver organoids, MEHP inhibited the TCA cycle, whereas in HepG2 cells, it upregulated both oxidative phosphorylation and TCA cycle (Fig. 6e). In terms of lipid metabolism, MEHP primarily promoted the oxidation and degradation of fatty acids, as evidenced by the upregulation of genes such as ACOX1, ACAA2, ACADVL, HADH, and ACSL, while concurrently inhibiting fatty acid biosynthesis, as indicated by the downregulation of genes including FASN, MCAT, ECHS1, HACD1, and MECR in liver organoids (Fig. 6f). In contrast, in HepG2 cells, genes related to fatty acid biosynthesis were also upregulated (Fig. 6f). Furthermore, the differential response of the

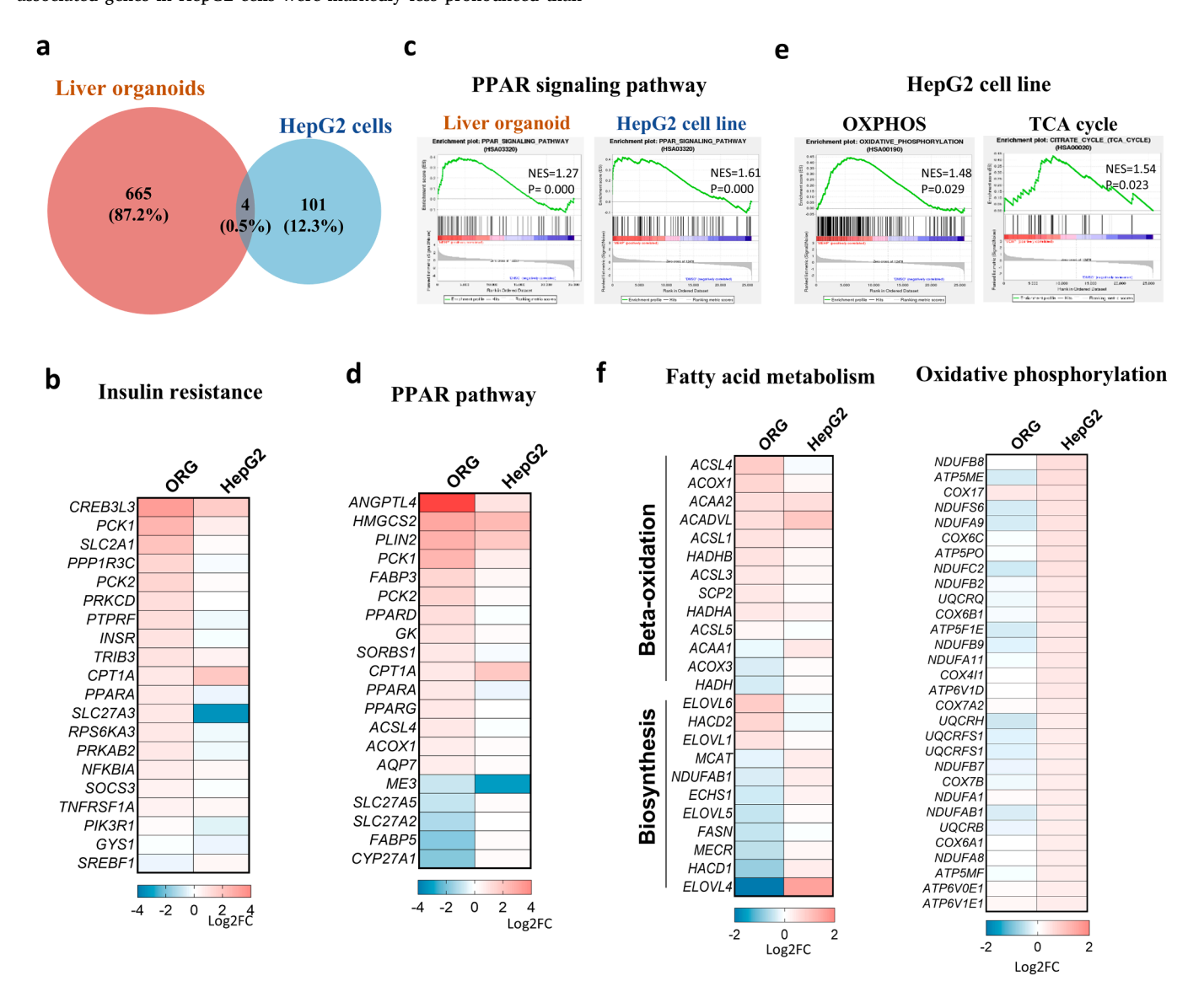


Fig. 6. Comparative analysis of human liver organoid and HepG2 cell models in response to MEHP. (a) Venn diagram showing the overlap in differentially expressed genes (DEGs) between liver organoids (ORG) and HepG2 cells treated with MEHP (50 μ M) for 48 h. (b) Comparison of the expression changes of insulin resistance-associated genes in liver organoids and HepG2 cells. (c) GSEA analysis highlighting the upregulation of the PPAR signaling pathway in both liver organoids and HepG2 cells. (d) Comparison of the expression changes of PPAR signaling pathway-related genes in liver organoids and HepG2 cells. (e) GSEA analysis highlighting the upregulation of oxidative phosphorylation (OXPHOS) and Tricarboxylic acid cycle (TCA) in HepG2 cells induced by MEHP. (f) Comparison of expression changes of genes associated with fatty acid metabolism and oxidative phosphorylation between liver organoids and HepG2 cells.

OXPHOS pathway between the two models was particularly evident. MEHP markedly suppressed OXPHOS gene expression in liver organoids but induced its upregulation in HepG2 cells (Fig. 6f). Collectively, these findings suggest that liver organoids exhibit heightened sensitivity to MEHP-induced activation of PPAR signaling pathway and disruption of glucose metabolism. Therefore, compared to the widely used HepG2 cell line, liver organoids may represent a more appropriate alternative model for evaluating the potential risks and elucidating the molecular mechanisms underlying phthalates-induced metabolic disorders, such as GDM.

4. Discussion

In this study, our data demonstrated that four phthalate metabolites (MBP, MEHP, MEP, and MBzP) are elevated in GDM patients, suggesting a potential link to GDM risk. The observed elevation in these compounds' levels may reflect greater exposure to phthalates in GDM patients and altered metabolism during pregnancy (Chen et al., 2023; Peng et al., 2024). This aligns with previous studies linking phthalate exposure to diabetes risk. For example, cross-sectional studies have reported associations between urinary phthalate metabolites and markers of glucose intolerance (James-Todd et al., 2022; Shaffer et al., 2019). However, the causality between phthalates and GDM and its underlying mechanisms remains unclear. Our findings on the metabolic disruptions induced by MEHP and MBP in human liver organoids suggest that phthalates may exacerbate hepatic lactate accumulation and insulin resistance, providing a mechanistic explanation for the health implication of phthalates exposure.

Numerous human and animal studies have shown that the developing male reproductive system is highly susceptible to DEHP's toxic effects (Agency for Toxic Substances and Disease Registry ATSDR Toxicological Profiles, 2022), and reproductive toxicity has long been the reference endpoint for estimating tolerable daily intake (TDI) of phthalates (Lambré et al., 2022). Nevertheless, emerging data indicates that metabolic systems might be more sensitive to certain phthalates than their reproductive toxicity (Silano et al., 2019). The liver is recognized as the primary target organ for the repeated-dose toxicity of DEHP in rodents (Li et al., 2021). But in adult human populations, it is to establish a causal link between metabolic dysfunction-associated steatotic liver disease (MASLD) and phthalate exposure (Gogola et al., 2025). PPAR activation in the liver by DEHP and its metabolites is well-documented in mice and rats (Rusyn and Corton, 2012; Rusyn et al., 2006). However, the varying sensitivity of PPARs in hepatocytes across different species poses a significant challenge to human health risk assessment (Foreman et al., 2021). Although some studies using HepG2 cells have shown DEHP induces hepatotoxicity, it is uncertain whether these cells can accurately replicate the normal hepatocyte phenotype and liver tissue microenvironment. In contrast, human liver organoids provide a more physiologically relevant model for studying the metabolic-disrupting effects of phthalates. Our results demonstrate that MEHP and MBP significantly altered glucose and lipid metabolism in liver organoids, which may offer scientific evidence for explaining GDM etiology.

RNA sequencing and HCI analysis using liver organoids have offered insights into the molecular mechanisms underlying the metabolic dysregulation by MEHP and MBP. Of particular significance, glycolysis/gluconeogenesis and the HIF-1 signaling pathway emerged as the most substantially altered KEGG pathways. The changes suggest a shift in hepatic energy metabolism toward glycolysis, potentially leading to the increased lactate production as observed in our experiments. The activation of the HIF-1 pathway corroborates the hypothesis that phthalates induce a hypoxic metabolic state (Li et al., 2024). HIF-1, a transcription factor stabilized under hypoxia, plays a crucial role in promoting glycolysis and inhibiting oxidative phosphorylation (Gonzalez et al., 2018). The upregulation of HIF-1 target genes, such as LDHA, which catalyzes the conversion of pyruvate to lactate, explains the observed

increase in lactate production. This metabolic shift not only disrupts glucose homeostasis but also contributes to metabolic acidosis, thereby exacerbating insulin resistance (DiNicolantonio and O'Keefe, 2021). Another key pathway highlighted by our analysis is the mTOR signaling pathway, which is closely associated with insulin resistance and metabolic disorders. Activation of mTOR can lead to increased glycolysis while suppressing insulin signaling (Saxton and Sabatini, 2017). Collectively, these results highlight the liver as a critical target organ for phthalate-induced metabolic disruption such as GDM.

The comparative analysis between liver organoids and HepG2 cells revealed significant differences in the response to phthalate metabolites. Our results suggest that liver organoids are more sensitive to the metabolic-disrupting effects of phthalates. The greater sensitivity of liver organoids may be attributed to their more physiologically-relevant structure and functions (Hendriks et al., 2024; Igarashi et al., 2025). For example, the expression changes of insulin resistance associated genes were more pronounced in liver organoids than in HepG2 cells. This highlights the importance of using liver organoids as a more appropriate model for studying the toxicological effects of phthalates on hepatic metabolism.

The clinical relevance of our findings lies in the potential for phthalate exposure to contribute to the rising prevalence of metabolic disorders (Chew et al., 2023). The observed metabolic disruptions in liver organoids, such as enhanced glycolysis and lactate production, suggest that phthalates may exacerbate insulin resistance and glucose intolerance. Given the widespread use of phthalates in consumer products and the difficulty in avoiding environmental exposure, our results emphasize the need for strategies to reduce phthalate exposure, particularly during pregnancy and other critical periods of metabolic vulnerability.

5. Limitations

Firstly, the cohort was recruited from a single geographic region of China; therefore, allele-frequency gradients, dietary patterns and other lifestyle factors may constrain external validity. For the organoid experiments, on one hand, the short-term treatment with MEHP and MBP cannot reproduce life-long, low-dose exposure in human population; on the other hand, the experimental concentrations were higher than human-relevant serum levels, which may overestimate the toxicological potency. In addition, only two individual metabolites (MBP and MEHP) were tested, whereas humans are concurrently exposed to complex phthalate mixtures that may act additively or synergistically; thus, the study may underestimate real-world risk. Finally, although hepatic metabolism was investigated, the multi-organ signalling network linking phthalate exposure to systemic insulin resistance remains incompletely mapped.

6. Conclusion

In conclusion, our study provides novel evidence linking phthalate exposure to GDM risk and elucidates the underlying mechanisms through which phthalates disrupt hepatic metabolism. The elevated levels of MBP and MEHP in GDM patients and their disruptive effects on glucose and lipid metabolism in liver organoids highlight the potential role of phthalates in GDM pathogenesis. Our findings underscore the importance of considering environmental exposures in the context of GDM prevention and management.

CRediT authorship contribution statement

Yuxin Wang: Software, Investigation. Xiaohong Wang: Supervision. Xiaobing Zhao: Supervision, Funding acquisition. Xudong Jia: Supervision. Xiaoning Ji: Investigation, Data curation. Miaoying Shi: Supervision, Data curation. Hongyang Cui: Supervision, Methodology. Huihui Liu: Writing – original draft, Supervision, Data curation. Yi

Wan: Supervision. Zhaojing Yang: Writing — original draft, Supervision, Data curation. Hui Yang: Writing — original draft, Supervision, Methodology, Funding acquisition, Data curation, Conceptualization. Yaru Tian: Writing — original draft, Investigation, Data curation. Shujing Yu: Supervision. Zhishen Zhuang: Writing — original draft, Investigation, Data curation.

Compliance with ethical standards

The GDM case-control study, which involved the use of human serum samples, was approved by the Ethics Committee of the Maternal and Child Health Hospital of Zaozhuang City (Approval Number: zfy-2023–69). All participants provided written informed consent prior to their inclusion in the study. The research was conducted in accordance with the Declaration of Helsinki.

Consent for publication

All authors have given their consent for submission of this content.

Declaration of Competing Interest

The authors declare that they have no known competing financial interests or personal relationships that could have appeared to influence the work reported in this paper.

Acknowledgments

This work was supported by the National Natural Science Foundation of China (Grants No. 82373625) and Key Technologies Research and Development Program (Grants No. 2023YFF1104103). We thank Prof. Chen Jin from Zaozhuang Maternal and Child Health Care Hospital for providing expert consultation in this study.

Appendix A. Supporting information

Supplementary data associated with this article can be found in the online version at doi:10.1016/j.ecoenv.2025.119305.

Data availability

Data will be made available on request.

References

- Agency for Toxic Substances and Disease Registry (ATSDR) Toxicological Profiles. (2022). (A. f. T. S. a. D. R. (US), Ed.). Agency for Toxic Substances and Disease Registry (US).
- Chen, W., He, C., Liu, X., An, S., Wang, X., Tao, L., Zhang, H., Tian, Y., Wu, N., Xu, P., Liao, D., Liao, J., Wang, L., Fang, D., Xiong, S., Liu, Y., Tian, K., Li, Q., Huang, J., Zhou, Y., 2023. Effects of exposure to phthalate during early pregnancy on gestational diabetes mellitus: a nested case-control study with propensity score matching. Environ. Sci. Pollut. Res. Int. 30 (12), 33555–33566. https://doi.org/10.1007/s11356-022-24454-y
- Chew, N.W.S., Ng, C.H., Tan, D.J.H., Kong, G., Lin, C., Chin, Y.H., Lim, W.H., Huang, D. Q., Quek, J., Fu, C.E., Xiao, J., Syn, N., Foo, R., Khoo, C.M., Wang, J.W., Dimitriadis, G.K., Young, D.Y., Siddiqui, M.S., Lam, C.S.P., Muthiah, M.D., 2023. The global burden of metabolic disease: Data from 2000 to 2019. e413 Cell Metab. 35 (3), 414–428. https://doi.org/10.1016/j.cmet.2023.02.003.
- Corton, J.C., Peters, J.M., Klaunig, J.E., 2018. The PPARα-dependent rodent liver tumor response is not relevant to humans: addressing misconceptions. Arch. Toxicol. 92 (1), 83–119. https://doi.org/10.1007/s00204-017-2094-7.
- DiNicolantonio, J.J., O'Keefe, J.H., 2021. Low-grade metabolic acidosis as a driver of insulin resistance. Open Heart 8 (2). https://doi.org/10.1136/openhrt-2021-001788
- Eberle, C., Stichling, S., 2022. Environmental health influences in pregnancy and risk of gestational diabetes mellitus: a systematic review. BMC Public Health 22 (1), 1572. https://doi.org/10.1186/s12889-022-13965-5.
- Filardi, T., Panimolle, F., Lenzi, A., Morano, S., 2020. Bisphenol A and phthalates in diet: an emerging link with pregnancy complications. Nutrients 12 (2), 525. https://doi. org/10.3390/nu12020525.

- Foreman, J.E., Koga, T., Kosyk, O., Kang, B.H., Zhu, X., Cohen, S.M., Billy, L.J., Sharma, A.K., Amin, S., Gonzalez, F.J., Rusyn, I., Peters, J.M., 2021. Species differences between mouse and human ppara in modulating the hepatocarcinogenic effects of perinatal exposure to a high-affinity human PPARa agonist in mice. Toxicol. Sci. 183 (1), 81–92. https://doi.org/10.1093/toxsci/kfab068.
- Fruh, V., Preston, E.V., Quinn, M.R., Hacker, M.R., Wylie, B.J., O'Brien, K., Hauser, R., James-Todd, T., Mahalingaiah, S., 2022. Urinary phthalate metabolite concentrations and personal care product use during pregnancy Results of a pilot study. Sci. Total Environ. 835, 155439. https://doi.org/10.1016/j.sci.toteny.2022.155439
- Gao, H., Zhu, B.B., Huang, K., Zhu, Y.D., Yan, S.Q., Wu, X.Y., Han, Y., Sheng, J., Cao, H., Zhu, P., Tao, F.B., 2021. Effects of single and combined gestational phthalate exposure on blood pressure, blood glucose and gestational weight gain: A longitudinal analysis. Environ. Int 155, 106677. https://doi.org/10.1016/j.envirt 2021 106677
- Gogola, T., Pitkänen, S., Huovinen, M., Laitinen, H., Küblbeck, J., 2025. Association between phthalate exposure and metabolic dysfunction-associated steatotic liver disease (MASLD) - systematic literature review. Environ. Res 273, 121186. https:// doi.org/10.1016/j.envres.2025.121186.
- Gonzalez, F.J., Xie, C., Jiang, C., 2018. The role of hypoxia-inducible factors in metabolic diseases. Nat. Rev. Endocrinol. 15 (1), 21–32. https://doi.org/10.1038/s41574-018-0096-z.
- Hendriks, D., Artegiani, B., Margaritis, T., Zoutendijk, I., Chuva de Sousa Lopes, S., Clevers, H., 2024. Mapping of mitogen and metabolic sensitivity in organoids defines requirements for human hepatocyte growth. Nat. Commun. 15 (1), 4034. https:// doi.org/10.1038/s41467-024-48550-4.
- Hendriks, D., Brouwers, J.F., Hamer, K., Geurts, M.H., Luciana, L., Massalini, S., López-Iglesias, C., Peters, P.J., Rodríguez-Colman, M.J., Chuva de Sousa Lopes, S., Artegiani, B., Clevers, H., 2023. Engineered human hepatocyte organoids enable CRISPR-based target discovery and drug screening for steatosis. Nat. Biotechnol. 41 (11), 1567–1581. https://doi.org/10.1038/s41587-023-01680-4.
- Hivert, M.F., Backman, H., Benhalima, K., Catalano, P., Desoye, G., Immanuel, J., McKinlay, C.J.D., Meek, C.L., Nolan, C.J., Ram, U., Sweeting, A., Simmons, D., Jawerbaum, A., 2024. Pathophysiology from preconception, during pregnancy, and beyond. Lancet 404 (10448), 158–174. https://doi.org/10.1016/s0140-6736(24) 00827-4.
- Huang, W., Pan, X.F., Tang, S., Sun, F., Wu, P., Yuan, J., Sun, W., Pan, A., Chen, D., 2023. Target exposome for characterizing early gestational exposure to contaminants of emerging concern and association with gestational diabetes mellitus. Environ. Sci. Technol. 57 (36), 13408–13418. https://doi.org/10.1021/acs.est.3c04492.
- Huch, M., Dorrell, C., Boj, S.F., van Es, J.H., Li, V.S., van de Wetering, M., Sato, T., Hamer, K., Sasaki, N., Finegold, M.J., Haft, A., Vries, R.G., Grompe, M., Clevers, H., 2013. In vitro expansion of single Lgr5+ liver stem cells induced by Wnt-driven regeneration. Nature 494 (7436), 247–250. https://doi.org/10.1038/nature11826.
- Igarashi, R., Oda, M., Okada, R., Yano, T., Takahashi, S., Pastuhov, S., Matano, M., Masuda, N., Togasaki, K., Ohta, Y., Sato, S., Hishiki, T., Suematsu, M., Itoh, M., Fujii, M., Sato, T., 2025. Generation of human adult hepatocyte organoids with metabolic functions (Online ahead of print). Nature. https://doi.org/10.1038/ 041596-075-09613;
- Jabato, F.M., Córdoba-Caballero, J., Rojano, E., Romá-Mateo, C., Sanz, P., Pérez, B., Gallego, D., Seoane, P., Ranea, J.A.G., Perkins, J.R., 2021. Gene expression analysis method integration and co-expression module detection applied to rare glucide metabolism disorders using ExpHunterSuite. Sci. Rep. 11 (1), 15062. https://doi.org/10.1038/s41598-021-94343-w.
- James-Todd, T.M., Chiu, Y.H., Messerlian, C., Mínguez-Alarcón, L., Ford, J.B., Keller, M., Petrozza, J., Williams, P.L., Ye, X., Calafat, A.M., Hauser, R., 2018. Trimester-specific phthalate concentrations and glucose levels among women from a fertility clinic. Environ. Health 17 (1), 55. https://doi.org/10.1186/s12940-018-0399-5.
- James-Todd, T.M., Meeker, J.D., Huang, T., Hauser, R., Ferguson, K.K., Rich-Edwards, J. W., McElrath, T.F., Seely, E.W., 2016. Pregnancy urinary phthalate metabolite concentrations and gestational diabetes risk factors. Environ. Int 96, 118–126. https://doi.org/10.1016/j.envint.2016.09.009.
- James-Todd, T., Ponzano, M., Bellavia, A., Williams, P.L., Cantonwine, D.E., Calafat, A. M., Hauser, R., Quinn, M.R., Seely, E.W., McElrath, T.F., 2022. Urinary phthalate and DINCH metabolite concentrations and gradations of maternal glucose intolerance. Environ. Int 161, 107099. https://doi.org/10.1016/j.envint.2022.107099.
- Kahn, L.G., Philippat, C., Nakayama, S.F., Slama, R., Trasande, L., 2020. Endocrine-disrupting chemicals: implications for human health. Lancet Diabetes Endocrinol. 8 (8), 703–718. https://doi.org/10.1016/s2213-8587(20)30129-7.
- Lambré, C., Barat Baviera, J.M., Bolognesi, C., Chesson, A., Cocconcelli, P.S., Crebelli, R., Gott, D.M., Grob, K., Lampi, E., Mengelers, M., Mortensen, A., Rivière, G., Steffensen, I.L., Tlustos, C., Van Loveren, H., Vernis, L., Zorn, H., Ahrens, B., Fabjan, E., Castle, L., 2022. Identification and prioritisation for risk assessment of phthalates, structurally similar substances and replacement substances potentially used as plasticisers in materials and articles intended to come into contact with food. Efsa J. 20 (5), e07231. https://doi.org/10.2903/ji.efsa.2022.7231.
- Li, X.L., Cai, X.Y., Ning, X., Liang, Y.Y., Hong, Y., Li, Q.M., Hu, D., Zheng, Y.Z., Cai, Y., Xu, T., Zhao, L.L., 2024. Role of sleep in asthenospermia induced by di (2-ethyl-hexyl) phthalate. Environ. Sci. Pollut. Res Int 31 (9), 13965–13980. https://doi.org/10.1007/s11356-024-32030-9
- Li, G., Zhao, C.Y., Wu, Q., Guan, S.Y., Jin, H.W., Na, X.L., Zhang, Y.B., 2021. Integrated metabolomics and transcriptomics reveal di(2-ethylhexyl) phthalate-induced mitochondrial dysfunction and glucose metabolism disorder through oxidative stress in rat liver. Ecotoxicol. Environ. Saf. 228, 112988. https://doi.org/10.1016/j. ecoenv.2021.112988.

- Lin, Y., Bai, M., Wang, S., Chen, L., Li, Z., Li, C., Cao, P., Chen, Y., 2022. Lactate is a key mediator that links obesity to insulin resistance via modulating cytokine production from adipose tissue. Diabetes 71 (4), 637–652. https://doi.org/10.2337/db21-0535.
- Mariana, M., Cairrao, E., 2023. The relationship between phthalates and diabetes: a review. Metabolites 13 (6), 746. https://doi.org/10.3390/metabo13060746.
- Martínez-Ibarra, A., Martínez-Razo, L.D., Vázquez-Martínez, E.R., Martínez-Cruz, N., Flores-Ramírez, R., García-Gómez, E., López-López, M., Ortega-González, C., Camacho-Arroyo, I., Cerbón, M., 2019. Unhealthy levels of phthalates and Bisphenol A in Mexican pregnant women with gestational diabetes and its association to altered expression of miRNAs involved with metabolic disease. Int. J. Mol. Sci. 20 (13), 3343. https://doi.org/10.3390/ijms20133343.
- McIntyre, H.D., Catalano, P., Zhang, C., Desoye, G., Mathiesen, E.R., Damm, P., 2019. Gestational diabetes mellitus. Nat. Rev. Dis. Prim. 5 (1), 47. https://doi.org/ 10.1038/s41572-019-0098-8.
- McIntyre, H.D., Kampmann, U., Dalsgaard Clausen, T., Laurie, J., Ma, R.C.W., 2024. Gestational diabetes: an update 60 years After O'Sullivan and Mahan. J. Clin. Endocrinol. Metab. 110 (1), e19–e31. https://doi.org/10.1210/clinem/dgae709.
- Peng, M.Q., Dabelea, D., Adgate, J.L., Perng, W., Calafat, A.M., Kannan, K., Starling, A.P., 2024. Associations of urinary biomarkers of phthalates, phenols, parabens, and organophosphate esters with glycemic traits in pregnancy: The Healthy Start Study. Environ. Res. 262 (Pt 1), 119810. https://doi.org/10.1016/j.envres.2024.119810.
- Petersen, M.C., Vatner, D.F., Shulman, G.I., 2017. Regulation of hepatic glucose metabolism in health and disease. Nat. Rev. Endocrinol. 13 (10), 572–587. https://doi.org/10.1038/nrendo.2017.80.
- Robledo, C.A., Peck, J.D., Stoner, J., Calafat, A.M., Carabin, H., Cowan, L., Goodman, J. R., 2015. Urinary phthalate metabolite concentrations and blood glucose levels during pregnancy. Int. J. Hyg. Environ. Health 218 (3), 324–330. https://doi.org/10.1016/i.iiheh.2015.01.005.
- Rusyn, I., Corton, J.C., 2012. Mechanistic considerations for human relevance of cancer hazard of di(2-ethylhexyl) phthalate. Mutat. Res 750 (2), 141–158. https://doi.org/ 10.1016/j.mrrev.2011.12.004.
- Rusyn, I., Peters, J.M., Cunningham, M.L., 2006. Modes of action and species-specific effects of di-(2-ethylhexyl)phthalate in the liver. Crit. Rev. Toxicol. 36 (5), 459–479. https://doi.org/10.1080/10408440600779065.
- Saxton, R.A., Sabatini, D.M., 2017. mTOR signaling in growth, metabolism, and disease. Cell 168 (6), 960–976. https://doi.org/10.1016/j.cell.2017.02.004.
- Schaffert, A., Karkossa, I., Ueberham, E., Schlichting, R., Walter, K., Arnold, J., Blüher, M., Heiker, J.T., Lehmann, J., Wabitsch, M., Escher, B.I., von Bergen, M., Schubert, K., 2022. Di-(2-ethylhexyl) phthalate substitutes accelerate human adipogenesis through PPARy activation and cause oxidative stress and impaired

- metabolic homeostasis in mature adipocytes. Environ. Int. 164, 107279. https://doi.org/10.1016/j.envint.2022.107279.
- Shaffer, R.M., Ferguson, K.K., Sheppard, L., James-Todd, T., Butts, S., Chandrasekaran, S., Swan, S.H., Barrett, E.S., Nguyen, R., Bush, N., McElrath, T.F., Sathyanarayana, S., 2019. Maternal urinary phthalate metabolites in relation to gestational diabetes and glucose intolerance during pregnancy. Environ. Int. 123, 588–596. https://doi.org/10.1016/j.envint.2018.12.021.
- Shapiro, G.D., Dodds, L., Arbuckle, T.E., Ashley-Martin, J., Fraser, W., Fisher, M., Taback, S., Keely, E., Bouchard, M.F., Monnier, P., Dallaire, R., Morisset, A., Ettinger, A.S., 2015. Exposure to phthalates, bisphenol A and metals in pregnancy and the association with impaired glucose tolerance and gestational diabetes mellitus: The MIREC study. Environ. Int. 83, 63–71. https://doi.org/10.1016/j.envint.2015.05.016.
- Silano, V., Barat Baviera, J.M., Bolognesi, C., Chesson, A., Cocconcelli, P.S., Crebelli, R., Gott, D.M., Grob, K., Lampi, E., Mortensen, A., Rivière, G., Steffensen, I.L., Tlustos, C., Van Loveren, H., Vernis, L., Zorn, H., Cravedi, J.P., Fortes, C., Tavares Poças, M.F., Castle, L., 2019. Update of the risk assessment of di-butylphthalate (DBP), butyl-benzyl-phthalate (BBP), bis(2-ethylhexyl)phthalate (DEHP), diisononylphthalate (DINP) and di-isodecylphthalate (DIDP) for use in food contact materials. Efsa J. 17 (12), e05838. https://doi.org/10.2903/j.efsa.2019.5838.
- Sweeting, A., Hannah, W., Backman, H., Catalano, P., Feghali, M., Herman, W.H., Hivert, M.F., Immanuel, J., Meek, C., Oppermann, M.L., Nolan, C.J., Ram, U., Schmidt, M.I., Simmons, D., Chivese, T., Benhalima, K., 2024. Epidemiology and management of gestational diabetes. Lancet 404 (10448), 175–192. https://doi.org/ 10.1016/s0140-6736(24)00825-0.
- Takeuchi, S., Iida, M., Kobayashi, S., Jin, K., Matsuda, T., Kojima, H., 2005. Differential effects of phthalate esters on transcriptional activities via human estrogen receptors alpha and beta, and androgen receptor. Toxicology 210 (2-3), 223–233. https://doi. org/10.1016/j.tox.2005.02.002.
- Tuculina, M.J., Perlea, P., Gheorghiță, M., Cumpătă, C.N., Dascălu, I.T., Turcu, A., Nicola, A.G., Gheorghiță, L.M., Diaconu, O.A., Valea, A., Ghemigian, A., Carsote, M., 2022. Diabetes mellitus: plasticizers and nanomaterials acting as endocrine-disrupting chemicals (Review). Exp. Ther. Med 23 (4), 288. https://doi.org/10.3892/etm.2022.11217.
- Wang, H., Chen, R., Gao, Y., Qu, J., Zhang, Y., Jin, H., Zhao, M., Bai, X., 2023. Serum concentrations of phthalate metabolites in pregnant women and their association with gestational diabetes mellitus and blood glucose levels. Sci. Total Environ. 857 (Pt 3), 159570. https://doi.org/10.1016/j.scitotenv.2022.159570.
- Yan, D., Jiao, Y., Yan, H., Liu, T., Yan, H., Yuan, J., 2022. Endocrine-disrupting chemicals and the risk of gestational diabetes mellitus: a systematic review and meta-analysis. Environ. Health 21 (1), 53. https://doi.org/10.1186/s12940-022-00858-8.